Bandwidth scaling of a phase-modulated continuous-wave comb through four-wave mixing in a silicon nano-waveguide

Yang Liu,[1,*] Andrew J. Metcalf,[1] Victor Torres Company,[1,2] Rui Wu,[1,3] Li Fan,[1,4] Leo T. Varghese,[1,4] Minghao Qi,[1,4] and Andrew M. Weiner[1,4]

[1]*School of Electrical and Computer Engineering, Purdue University, 465 Northwestern Avenue, West Lafayette, Indiana 47907-2035, USA*

[2]*Currently at Department of Microtechnology and Nanoscience (MC2), Chalmers University of Technology, 41296 Gothenburg, Sweden*

[3]*Currently at Intel Corporation, 2501 NW 229th Avenue, Hillsboro, Oregon 97124, USA*

[4]*Birck Nanotechnology Center, Purdue University, 1205 West State Street, West Lafayette, Indiana 47907, USA*

**Corresponding author: yangliu@purdue.edu*

Received August 18, 2014; revised October 13, 2014; accepted October 14, 2014; posted October 15, 2014 (Doc. ID 221117); published November 11, 2014

We demonstrate an on-chip four-wave mixing (FWM) scheme in a silicon nanowaveguide to scale the bandwidth of a frequency comb generated by phase modulation of continuous-wave (CW) lasers. The FWM process doubles the bandwidth of the initial comb generated by the modulation of a CW laser. For example, a wavelength-tunable frequency comb with >100 comb lines spaced by 10 GHz within a bandwidth of 5 dB is generated.

OCIS codes: (190.4390) Nonlinear optics, integrated optics; (060.5060) Phase modulation; (060.5625) Radio frequency photonics.

http://dx.doi.org/10.1364/OL.39.006478

Strong sinusoidal phase modulation (PM) of a continuous-wave (CW) laser can create multiple sidebands to form a frequency comb [1,2]. This technique enables the creation of high-repetition-rate combs with stable optical frequencies while allowing for the independent tuning of the repetition rate and optical center frequency. These attributes, combined with the simplicity of the technique, make it an ideal candidate for applications in optical communications [3], radio-frequency (RF) photonics [4], and optical arbitrary waveform generation [5]. By PM alone, the spectral lines suffer from significant line-to-line amplitude variations, i.e., poor spectral flatness. The spectral flatness of the comb can be improved considerably by adding an intensity modulator (IM) in series with the PM [6,7]. In this scheme, the IM acts to carve out a flat-topped pulse train from the CW source, whereas the phase modulator introduces a quadratic phase on each pulse (thus acting as a time lens [8]). When correctly aligned, the carved pulse will coincide with the cusp of the PM at the point where the chirp imposed is almost linear, yielding a flatter spectral profile. This process can be interpreted in terms of time-to-frequency mapping [9]: if the chirping is sufficiently large, the envelope of the optical spectrum will become a scaled replica of the intensity pulse [10]. In many applications, increasing the bandwidth of the combs is also desirable. However, the bandwidth of the combs generated in this IM–PM scheme is limited due to the bandwidth and RF power-handling capability of the PM. Of course, by placing several phase modulators in tandem, larger bandwidths can be achieved (see, e.g., [11,12]). Another method involves first compressing the comb to a short pulse and then using nonlinear propagation in a dispersion-decreasing or highly nonlinear fiber (HNLF) to broaden the spectrum [13–15].

Our group has also demonstrated a method that achieved simultaneous bandwidth enhancement and improved flatness by exploiting four-wave mixing (FWM) in a HNLF [16]. In this method, two optical frequency combs centered at different frequencies, ω_1 and ω_2 (with $\omega_2 > \omega_1$), are mixed in a HNLF. Initially, each comb had a narrow bandwidth and poor flatness. However, after traveling through a cascade of FWM processes, new frequency combs that exhibit enhanced spectral width and flatness can be generated. For example, when properly phase-matched, the complex envelope of the Nth-order higher-frequency sideband centered at $(N+1)\ \omega_2 - N\omega_1$ will be proportional to

$$[e_2(t)]^{N+1}[e_1^*(t)]^N, \tag{1}$$

where $e_1(t)$ and $e_2(t)$ denote the complex field envelopes of the seed combs centered at ω_1 and ω_2, respectively. The frequency-converted signal will display an equivalent modulation index, increased by a factor of $2N+1$, provided the phase conjugation in $e_1(t)$ is properly managed [16].

Recently, several groups have investigated nonlinear processes in silicon waveguides, such as parametric amplification [17], Raman amplification [18], and FWM [19], which provide very high nonlinearity in a chip-based geometry. These devices have been proven to be practical in optical signal-processing applications, which require broadband wavelength conversion [20–22]. In this report, we utilize on-chip FWM to introduce a more compact and flexible scheme for the spectral broadening of a frequency comb. This technique, based on principles similar to [16], allowed us to achieve >100 lines at 10 GHz spacing within a bandwidth of 5 dB.

Figure 1 shows the experimental setup. This setup is different from the setup of [16] in three aspects. First, the 100 m of HNLF is replaced by a silicon nanowaveguide, which is only 1 cm in length. Second, the

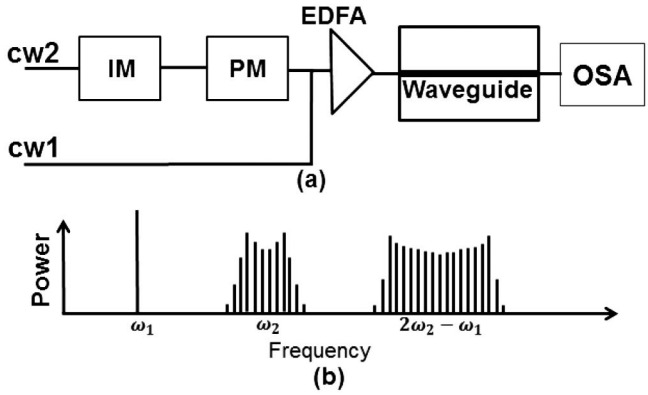

Fig. 1. (a) Experimental setup. CW, continuous-wave laser; IM, intensity modulator; PM, phase modulator; EDFA, high power erbium-doped fiber amplifier; OSA, optical spectrum analyzer; and (b) bandwidth scaling of the CW comb.

dispersion of the silicon chip can be tailored by engineering the waveguide cross-section geometry, which in turn increases the conversion bandwidth [20,21]. Finally, the signal centered at ω_1 will not be modulated, but instead will be directly combined with the second CW. In this case, the initial fields are given by $e_1(t) \sim 1$ and $e_2(t) \sim a(t)\exp[j\phi(t)]$, where $a(t)$ is the amplitude introduced by the IM and $\phi(t)$ is the phase introduced by the PM stage. Two inputs are mixed to produce a new first-order FWM component at $2\omega_2 - \omega_1$, given by $e_2^2(t)e_1^*(t) = a(t)^2\exp[2j\phi(t)]$. This indicates the new comb's bandwidth is roughly doubled with respect to the signal centered around ω_2. Compared to [16], this setup is more compact and flexible, although it comes at the expense of a reduction in the achievable bandwidth scaling. The reason behind these differences is that in [16], the signal centered at ω_1 first goes through an IM and is then combined with the second CW input centered at ω_2, after which both signals enter the PM, followed by a dispersive element. The role of the dispersive element was to delay the modulated signal by half a RF period. For this, the length L of the dispersive element must satisfy $D \cdot L \cdot \Delta\lambda = \frac{T_{\text{rep}}}{2}$, where D is the dispersion parameter of the dispersive element, $\Delta\lambda$ is the wavelength difference between the two CW inputs, and T_{rep} is the period of the RF modulation. This delay effectively performs a π phase shift to the field envelope term $e_1^*(t)$ in Eq. (1) to ensure that the PMs on the two fields are additive during the FWM process, rather than acting to cancel. Although this approach will effectively enhance the bandwidth by a factor of three for first-order mixing terms (50% higher than achieved with our current scheme), the dispersion (denoted as $D \cdot L$) must be changed in accordance with the changes in $\Delta\lambda$ or T_{rep}. Therefore, wavelength or repetition rate tunability is compromised.

Our silicon waveguide was patterned with electron-beam lithography on a silicon-on-insulator wafer. We designed the cross-section geometry so that it had a zero group velocity dispersion (GVD) wavelength within the C-band for quasi-TM polarization. The geometry was 800 nm in width by 250 nm in thickness. The two ends of the waveguide were inversely tapered to 100 nm, allowing light to be coupled in and out through a fiber taper. The end of the waveguide is followed by a U-groove to stabilize the fiber for high-power applications. The above setup provided a fiber-to-fiber loss of –8 dB, which includes the coupling and propagation losses. The propagation loss for our silicon waveguide was estimated to be about 3.5 dB/cm [23]. Finally, the nonlinear parameter was calculated to be in the order of 10^{-1} [rad/(W · cm)], three orders of magnitude higher than the HNLF in [16].

We first tested our waveguide with CW input for both pump and probe; the measured FWM spectrum at the nano-waveguide's output is given in Fig. 2(a), which shows a –19 dB conversion efficiency (defined as the idler to probe power ratio at the chip's output) when the pump power is 200 mW. At this power level, the waveguides sometimes get damaged after several hours of operation. We also measured the conversion efficiency spectrum of this waveguide. The result for pumping at 1550 nm is given in Fig. 2(b). We can achieve a relatively broad and flat conversion efficiency (>100 nm, <5 dB variation) when pumping at 1550 nm. Since the FWM conversion bandwidth is inversely proportional to the square root of the product of the interaction length and the GVD [24], this means that the zero dispersion point of the waveguide is very close to 1550 nm. The measurement limit in these experiments is given by the tuning range of the probe laser (1460–1580 nm). In our context, this means that the two frequency combs can be placed significantly further apart and generate broader combs operating at high repetition rates. It is worth noting that simultaneous broadband and flat conversion

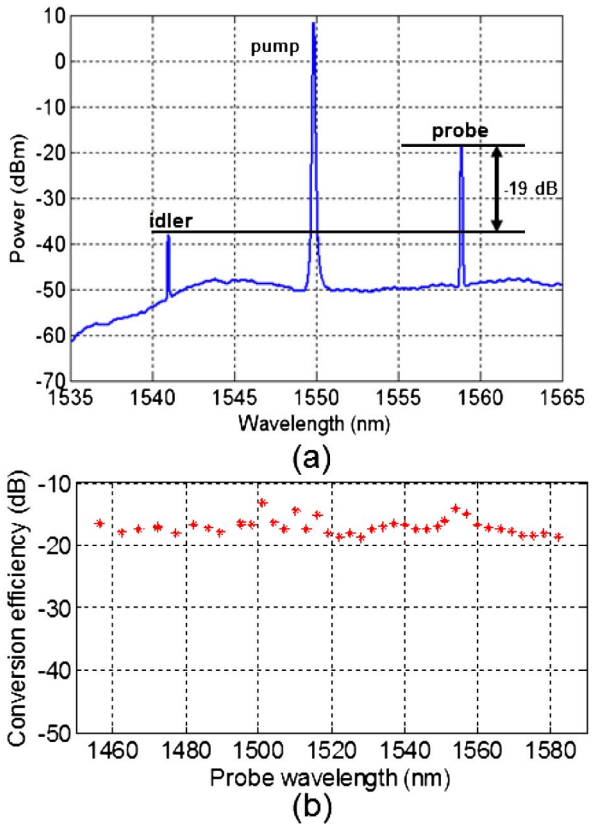

Fig. 2. (a) Spectrum for the FWM with CW inputs and (b) FWM conversion efficiency spectrum pumping at 1550 nm.

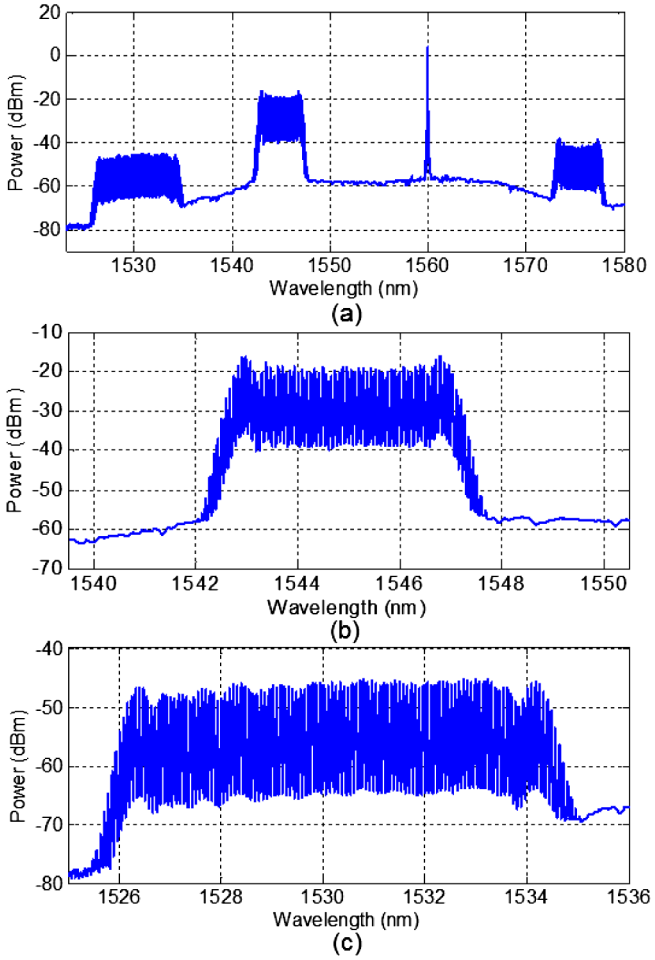

Fig. 3. (a) Output spectrum of the waveguide and (b), (c) zoomed-in view of the initial comb spectrum and the comb generated after FWM interaction, respectively.

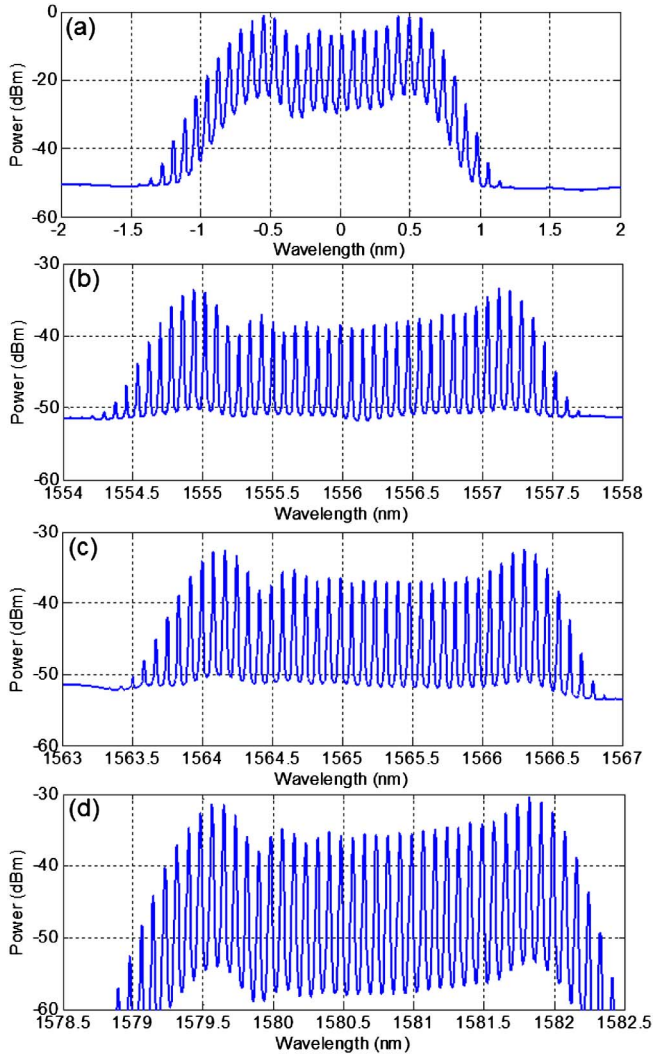

Fig. 4. Wavelength tuning of FWM generated frequency combs. (a) Input spectrum of the PM-IM comb. Output spectra of the comb with different wavelength separation between two CW lasers. The wavelength separation of the two inputs are 5, 10, and 20 nm, for (b), (c), and (d), respectively.

efficiency can be achieved for any pumping wavelength within the erbium-doped fiber amplifier gain bandwidth, allowing our input frequency to be chosen anywhere within this range.

We demonstrated our technique using a high-power frequency-tunable electro-optic comb source, which was comprised of 3 phase modulators and 1 IM. The performance details of this light source can be found in [12]. Our FWM results are shown in Fig. 3. The input frequency comb is centered at 1545 nm with a 10-GHz repetition rate and is comprised of about 55 lines at 5-dB bandwidth, as shown in Fig. 3(a). The input unmodulated CW is centered at 1560 nm. As expected, the FWM generated near 1530 nm has more than 100 lines in a 5-dB bandwidth. The small asymmetry and dips visible in the FWM term are likely caused by the conversion efficiency variations, as indicated in Fig. 1(b). This could be optimized by a more careful engineering of waveguide dispersion.

We now illustrate the wavelength-tuning capabilities of the broadened FWM combs. Here, the seed is instead synthesized using a simpler comb generator consisting of a single IM and single PM with 10 GHz repetition rate [spectrum shown in Fig. 4(a)]. The wavelength separation between the CW and seed comb is continuously varied, keeping their wavelengths centered near 1550 nm i.e., $(\lambda_1 + \lambda_2)/2 \approx 1550$ nm. Figures 4(b)–4(d) illustrate the first generated FWM sideband when the spacing between the input CW waveform and seed comb is set to 5, 10, and 20 nm, respectively. The bandwidth of the comb generated through FWM is again roughly twice that of the seed comb and remains approximately constant as it is tuned.

In the quest for a fully integrated system, we note the recent advances in hybrid silicon-organic electro-optic comb generators [25] and erbium waveguide amplifiers [26] developed in a silicon-on-insulator platform.

In summary, we have demonstrated a simple on-chip scheme to scale the bandwidth of a phase and intensity modulated CW comb. Compared to the previous nonlinear optical fiber scheme [16], our generated combs exhibit comparable bandwidth (>1 THz) and good flatness (>100 lines within 5-dB bandwidth). What sets our scheme apart is the added flexibility and compactness.

This project was supported in part by the Naval Postgraduate School under grant N00244-09-1-0068 and by the

National Science Foundation under grants ECCS-0925759 and ECCS-1102110. Victor Torres-Company gratefully acknowledges funding from the Swedish Research Council (VR).

References

1. H. Murata, A. Morimoto, T. Kobayashi, and S. Yamamoto, IEEE J. Sel. Top. Quantum Electron. **6**, 1325 (2000).
2. V. Torres-Company and A. M. Weiner, Laser Photon. Rev. **8**, 368 (2014).
3. T. Ohara, H. Takara, T. Yamamoto, H. Masuda, T. Morioka, M. Abe, and H. Takahashi, J. Lightwave Technol. **24**, 2311 (2006).
4. V. R. Supradeepa, C. M. Long, R. Wu, F. Ferdous, E. Hamidi, D. E. Leaird, and A. M. Weiner, Nat. Photonics **6**, 186 (2012).
5. Z. Jiang, C. B. Huang, D. E. Leaird, and A. M. Weiner, Nat. Photonics **1**, 463 (2007).
6. M. Fujiwara, M. Teshima, J. Kani, H. Suzuki, N. Takachio, and K. Iwatsuki, J. Lightwave Technol. **21**, 2705 (2003).
7. T. Otsuji, M. Yaita, T. Nagatsuma, and E. Sano, IEEE J. Sel. Top. Quantum Electron. **2**, 643 (1996).
8. B. H. Kolner and M. Nazarathy, Opt. Lett. **14**, 630 (1989).
9. J. Azaña, Opt. Commun. **217**, 205 (2003).
10. V. Torres-Company, J. Lancis, and P. Andres, Opt. Lett. **33**, 1822 (2008).
11. A. Ishizawa, T. Nishikawa, A. Mizutori, H. Takara, H. Nakano, T. Sogawa, A. Takada, and M. Koga, Opt. Express **19**, 22402 (2011).
12. A. J. Metcalf, V. Torres-Company, D. E. Leaird, and A. M. Weiner, IEEE J. Sel. Top. Quantum Electron. **84**, 3500306 (2013).
13. C. B. Huang, S. G. Park, D. E. Leaird, and A. M. Weiner, Opt. Express **16**, 2520 (2008).
14. R. P. Scott, N. K. Fontaine, J. P. Heritage, B. H. Kolner, and S. J. B. Yoo, in *Optical Fiber Communication Conference and Exposition and the National Fiber Optic Engineers Conference* (2007), paper OWJ3.
15. B. P.-P. Kuo, E. Myslivets, V. Ataie, E. G. Temprana, N. Alic, and S. Radic, J. Lightwave Technol. **31**, 3414 (2013).
16. V. R. Supradeepa and A. M. Weiner, Opt. Lett. **37**, 3066 (2012).
17. M. A. Foster, A. C. Turner, J. E. Sharping, B. S. Schmidt, M. Lipson, and A. L. Gaeta, Nature **441**, 960 (2006).
18. R. Claps, D. Dimitropoulos, V. Raghunathan, Y. Han, and B. Jalali, Opt. Express **11**, 1731 (2003).
19. H. Fukuda, K. Yamada, T. Shoji, M. Takahashi, T. Tsuchizawa, T. Watanabe, J. Takahashi, and S. Itabashi, Opt. Express **13**, 4629 (2005).
20. A. C. Turner-Foster, M. A. Foster, R. Salem, A. L. Gaeta, and M. Lipson, Opt. Express **18**, 1904 (2010).
21. R. K. W. Lau, M. Menard, Y. Okawachi, M. A. Foster, A. Turner-Foster, R. Salem, M. Lipson, and A. L. Gaeta, Opt. Lett. **36**, 1263 (2011).
22. H. Ji, M. Pu, H. Hu, M. Galili, L. K. Oxenlowe, K. Yvind, J. M. Hvam, and P. Jeppesen, J. Lightwave Technol. **29**, 426 (2011).
23. H. Shen, L. Fan, J. Wang, J. C. Wirth, and M. Qi, IEEE Photon. Technol. Lett. **22**, 1174 (2010).
24. M. E. Marhic, N. Kagi, T. K. Chiang, and L. G. Kazovsky, Opt. Lett. **21**, 573 (1996).
25. C. Weimann, P. C. Schindler, R. Palmer, S. Wolf, D. Bekele, D. Korn, J. Pfeifle, S. Koeber, R. Schmogrow, L. Alloatti, D. Elder, H. Yu, W. Bogaerts, L. R. Dalton, W. Freude, J. Leuthold, and C. Koos, Opt. Express **22**, 3629 (2014).
26. J. D. B. Bradley and M. Pollnau, Laser Photon. Rev. **5**, 368 (2011).